journal

J. Am. Ceram. Soc., 73 [3] 477–489 (1990)

Electronic Band Structure of Al_2O_3, with Comparison to AlON and AlN

Roger H. French*

Central Research and Development,
E. I. du Pont de Nemours & Company, Inc.,
Wilmington, Delaware 19880

As the uses of Al_2O_3 and other ceramics expand into new and more demanding applications, it is increasingly important to understand their electronic structure and its relationship to properties. However, compared with metals, semiconductors, or alkali halides, our understanding of the electronic structure of ceramic materials is limited. There has been much recent progress in our understanding of the electronic structure of Al_2O_3, based on the applications of new experimental and theoretical methods. Vacuum ultraviolet spectroscopy and valence band photoemission spectroscopy coupled with pseudofunction band structure methods provide a comprehensive approach to study a wide variety of electronic structure issues of importance to ceramic materials. The high-temperature electronic structure and its role in determining the high-temperature, intrinsic, electronic conductivity gives us the ability to evaluate high-temperature conductivity data, and supports the conclusion that Al_2O_3 is predominantly an electronic conductor at high-temperatures. The strain dependence of the electronic structure, as embodied in the deformation potentials, provides a simple method to determine surface stresses and strains. The variation of the electronic structure in the family Al_2O_3–AlON–AlN demonstrates the changes associated with the valence band chemistry of changing the anion from oxygen to nitrogen, and the bonding from mixed ionic–covalent in the direction of greater covalency. These changes in the anion valence bands lead to dramatic changes in the atomic and electronic nature of room-temperature bimaterial interface formation for copper to Al_2O_3 or AlN. The application of this new methodology to develop our perspective on electronic structure and apply it to problems associated with temperature, stress, composition, or interface formation can improve our understanding of many critical questions in ceramics. [Key words: alumina, electronic structure, spectroscopy, bonding, band structure.]

T. O. Mason—contributing editor

Manuscript No. 198264. Received June 30, 1989; approved September 8, 1989.

*Member, American Ceramic Society.

I. Introduction

DURING the past five years there has been a rapid development of our understanding of the electronic band structure of Al_2O_3.[1-4] Sophisticated applications of Al_2O_3 have motivated such studies, while new experimental and theoretical techniques have overcome the difficulties associated with studies of the electronic structure of ceramic materials. Al_2O_3 is a highly insulating material characterized by mixed ionic and covalent bonding, a limited range of atomic nonstoichiometry, a large band gap energy, and concomitant low concentrations of both ionic defects and electronic carriers. It is a mixed electronic–ionic conductor where low concentrations of electronic and ionic defects compete in determining the defect chemistry and related properties. The electronic structure is the context in which electronic defects are created, and also governs the oxidation and reduction of the ionic defects. In addition, the electronic structure governs the electron transfer and sharing responsible for bond formation at bimaterial interfaces such as Cu–Al_2O_3. These examples serve to highlight the fun-

Roger H. French has been a member of the Central Research Department of E. I. du Pont de Nemours & Company since 1985. His work at Du Pont has dealt principally with the electronic structure of ceramics and optical materials, and the development of new optical and vacuum ultraviolet spectroscopic techniques for electronic structure studies. His work has focused on the effects of temperature, composition, defects, and stress. He is currently working on defects in spinel, phase stabilization of ZrO_2, and phosphate and borate nonlinear optical crystals. In 1985 he was a postdoctoral associate in the Materials Science Department at Massachusetts Institute of Technology. He received his PhD in Materials Science in 1985 from MIT where his thesis work was on high-temperature electronic structure and conductivity of α-Al_2O_3. He received his BS in materials science from Cornell University in 1979.

review

damental role the band structure plays in determining the properties of Al_2O_3.

In this paper we review the techniques which together represent a comprehensive methodology for the study of the electronic structure of Al_2O_3. These are optical and photoelectron spectroscopies coupled with theoretical band structure calculations. We then present our current understanding of the room-temperature intrinsic band structure of Al_2O_3, and some new results on the high-temperature electronic structure, including the causes and effects of the temperature dependence of the electronic structure and the implications for the high-temperature conductivity of Al_2O_3. The strain dependence of the electronic structure gives rise to a simple method of measuring surface layer stresses in Al_2O_3. Finally, we contrast the band structure of the relatively ionic Al_2O_3 with the more covalent AlN and the implications this has for atomic bonding at copper–ceramic bimaterial interfaces.

Polarons and Optical and Thermal Band Gaps

The charge of a single electron in Al_2O_3 is relatively localized in real space, and optical excitation above the band gap energy, to create a free electron in the conduction band, corresponds to a charge transfer from oxygen to Al. This localized charge carrier, and the associated redistribution of charge, will cause an electrostatic relaxation of the neighboring Al^{3+} and O^{2-} ions, creating a lattice polarization field around the carrier; this is the formation of a polaron.[14,15] The lattice polarization serves to lower the energy of the polaron relative to the band electron. If the electron charge is distributed over 1 to 10 nm (10 to 100 Å), for example, then the electrostatic attraction to the ions is relatively weak, and only electronic charge redistribution occurs on the affected ions. This produces a large polaron, an electron whose polarization field only arises from electronic relaxation of the lattice; it will behave as a band carrier with an increased effective mass. If instead the charge of the electron is more highly localized, over 0.2 to 0.4 nm (2 to 4 Å), for example, then the electrostatic interaction with the ions is much greater and leads to both electronic and nuclear relaxation of the neighboring ions. This is called a small polaron. The resulting carrier is effectively trapped by the ionic relaxation and can only move in the lattice by a thermally activated process.

VUV or visible spectroscopy probes the excitations of a material at optical frequencies (10^{15} Hz) and therefore cannot probe the lower frequency (10^{12} Hz) phonon or lattice relaxation effects on the electronic structure. Optical excitations therefore create band electrons, whereas high-temperature thermal processes, which occur in the slower time scale of the lattice vibrations, lead to the direct creation of polarons. The optical band gap energy therefore corresponds to the creation of band electrons, whereas the thermal band gap energy corresponds to reduced energy required for direct formation of polarons. The quantity which relates the optical and thermal band gap energies is Δ, the lattice stabilization energy, or Stokes shift, of the polaron. Thermal energies for transitions must be equal to or less than the corresponding optical values.

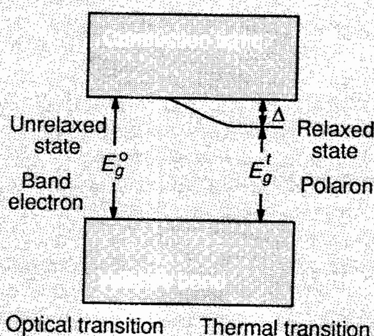

$$E_g^t = E_g^o - \Delta$$

An optical excitation above the optical band gap energy E_g^o will lead to the creation of a free electron in the conduction band, whereas a thermal excitation above the thermal band gap energy E_g^t will lead to the direct formation of a large polaron in Al_2O_3. The relationship between the optical and thermal band gap energies is determined by the lattice stabilization energy, Δ, of the polaron.

II. Methods and Results

(1) Optical Spectroscopy

Optical spectroscopy has typically been one of the first methods applied in studying the electronic structure of materials.[5-8] Optical transmission measurements probe the fundamental absorption edge and determine the optical band gap energy. Reflectance measurements are useful for probing interband transitions lying at higher energies, where the material is opaque. Reflectance measurements also probe many-body excitations, such as excitons (bound electron-hole pairs), providing a valuable probe of how electrons and holes interact in the lattice. In general, the ionic nature of Al_2O_3 results in an upper valence band derived from the O 2*p* states and a conduction band derived from the Al 3*s* and 3*p* states, with transitions seen in the reflectance corresponding to valence-to-conduction band transitions. For large band gap ceramic materials, normal optical spectroscopy techniques are limited, since air absorbs at 6 eV and windowed vacuum ultraviolet (VUV) light sources stop at 11 eV. VUV techniques[9,10] are required to span the energy range necessary to probe the valence-to-conduction band transitions of the intrinsic electronic structure. Therefore, optical spectroscopy results are less readily available for the electronic structure of ceramics than for smaller band gap materials. We have recently developed a laser plasma light source (LPLS) and are performing high-energy (2 to 40 eV) VUV reflectance measurements.[11,12] These new experimental and analytical capabilities, uniquely suited to ceramics, will further extend our understanding of the electronic structure of ceramics. VUV spectroscopy over a sufficiently wide energy range (5 to 40 eV for Al_2O_3) allows one to exhaust the transitions of the intrinsic electronic structure and to the determine the high-frequency dielectric constant and optical properties from Kramers–Kronig analysis,[13] providing quantitative electronic structure information.

The room-temperature VUV reflectance of single-crystal Al_2O_3 for light polarized perpendicular and parallel to the *c* axis is shown in Fig. 1. Peak 1, at 9 eV, arises from excition formation and is closely associated with the band gap of Al_2O_3. Peak 2, at approximately 12.6 eV, is due to direct interband transitions and shows anisotropic features. Al_2O_3 becomes opaque at the transmission cutoff of 8.8 eV, corresponding to the optical band gap energy. At 7 eV a shoulder is seen in the transmission of these nominally undoped crystals, which is due to a charge transfer transition from the chromium impurities which are present at parts-per-million lev-

els in these crystals. From the reflectance and transmission we can determine the absorption coefficient of Al_2O_3 in the band gap region as shown in Fig. 2.[16]

Wide energy range light sources, such as the LPLS or synchrotron radiation, allow the determination of the complete optical properties encompassing all valence-to-conduction band transitions. The reflectance of basal plane α-Al_2O_3 from 5 to 40 eV, acquired with the LPLS and shown in Fig. 3(A), is high from the band gap up to about 24 eV where it falls off rapidly because of the exhaustion of the upper valence-to-conduction band transitions. The peak seen at 32 eV arises from transitions from the O 2*s* lower valence band to the conduction band. Using Kramers–Kronig analysis, we can calculate the complex dielectric constant $\boldsymbol{\varepsilon} = \varepsilon_1 + i\varepsilon_2$, which demonstrates the independent effects of absorption and dispersion, and the optical conductivity (defined as $\sigma_1 = E\varepsilon_2$, where E is energy (as shown in Fig. 3(B)), which is proportional to the number of electronic interband transitions. These data can be used for analytical critical point analysis[17] to experimentally identify the energies of individual band-to-band transitions of the electronic structure,[4] and optical sum rule analysis[18] to determine the number of valence electrons involved in different transitions.

(2) Valence Band X-ray Photoemission Spectroscopy

Valence band X-ray photoemission spectroscopy (VBXPS) is used to determine the density of occupied valence band states in a material.[19] The penetration depth is about 10 nm (100 Å), and the results can be considered representative of the bulk valence states. Typically fracture surfaces of the ceramic, created in situ under ultrahigh vacuum (UHV) conditions, are used to avoid surface contamination, and low-energy electrons from a flood gun are used to overcome surface charging. Ultraviolet photoemission spectroscopy (UPS) is another method that uses lower energy VUV excitation to determine valence electron energies; it is therefore a more surface sensitive probe.

The experimentally determined valence band density of states (DOS) of Al_2O_3 is shown in Fig. 4, and it is compared with the calculated total and atomic partial DOS. We can see the two peaks in the upper valence band, which are the sources of the electrons whose transitions are measured in the VUV in the region above the band gap energy (8.8 to 24 eV). In addition there is a peak at -20 eV below the valence band maximum arising from the O 2*s* lower valence band. The region between the upper and lower valence bands is referred to as the ionicity gap, and the lack of any electronic states in this region is a demonstration of the ionicity of the material.

(3) Band Structure Calculations

The pseudofunction band structure method (PSF),[20-22] used for the calculations discussed here, is a first-principles method using no empirical potentials or parameters. It requires as input only the atomic positions of the atoms and their atomic numbers. The cation *sp*³*d*⁵ and anion *sp*³ orbitals are used as the basis set for the calculation, and the calculation is iterated to arrive at a self-consistent set of one-electron energies. These one-electron calculations cannot at present calculate quasi particles, or many-body effects, such as polarons or excitons, nor do they allow atomic relaxations from the input positions, as is done in pair-potential-based molecular dynamics calculations. Recent schemes such as the ab initio molecular dynamics method of Car and Parrinello[23] are attempts to bring together the molecular dynamics approach of moving atoms and density functional one-electron calculations and may see increasing importance in the coming years.

The PSF method, similar to most modern band structure methods, makes use of density functional theory, as embodied in the local density approximation (LDA).[28] The LDA states that the energy of a one-electron state is only determined by the potential from other electrons and nuclei in a local area. This approximation has reduced the complexity of band structure calculations and, coupled with the computational power of supercomputers, has made possible band structure calculations on very complex, low-symmetry systems, such as ceramics. LDA calculations are fundamentally ground-state calculations and, therefore, tend to underestimate the band gap energy since this energy corresponds to a transition to a higher-energy excited state of the solid.[29] LDA calculations do not consider many-body effects or the effects of the nonlocal redistribution of charge associated with excitations. Although the band gaps are typically underestimated in the calculations, bandwidths and the density of valence and conduction band states are well represented in LDA calculations.

The **k**-space band diagram for Al_2O_3, calculated using room-temperature bond lenghts, is shown in Fig. 5(A). The valence and conduction bands are separated by a calculated band gap of 6.3 eV. From sampling the number of electronic states in **k** space at each energy, one can determine the valence and conduction band DOS shown in Fig. 5(B). The DOS can be decomposed into its atomic partial DOS to show the atomic origins of the electronic states at different energies.

III. Room-Temperature Band Structure

The room-temperature band gap of Al_2O_3 is 8.8 eV, as can be seen in the transmission cutoff (Fig. 1(C)) or the dramatic increase in the absorption coefficient (Fig. 2). This is the optical band gap ener-

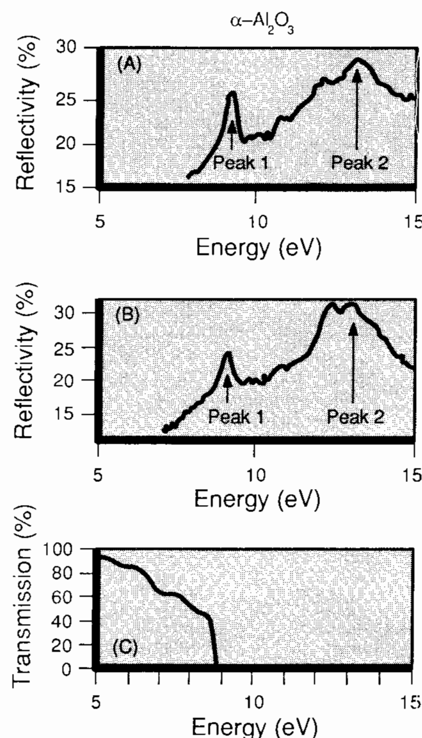

Fig. 1. VUV reflectivity for **E** polarized (A) perpendicular and (B) parallel to the *c* axis, and (C) the VUV transmission cutoff of single-crystal α-Al_2O_3 at room temperature.

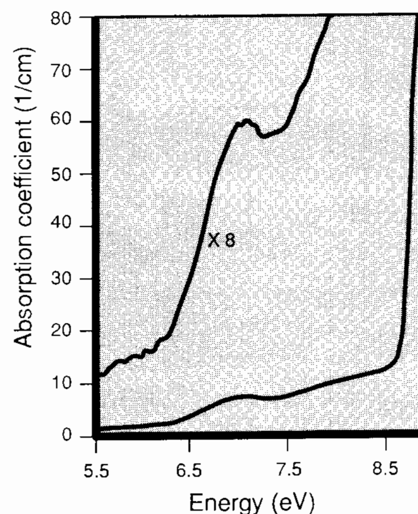

Fig. 2. Absorption coefficient of single-crystal α-Al_2O_3 at room temperature.[16]

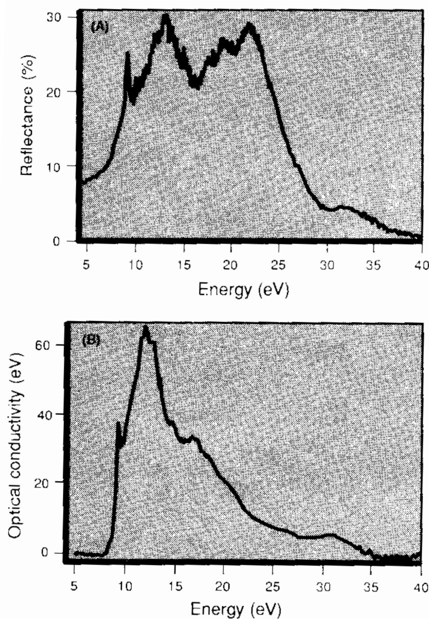

Fig. 3. (A) VUV reflectivity and (B) optical conductivity ($\sigma_1 = E\varepsilon_2$, where ε_2 is the imaginary part of the dielectric constant) of single-crystal α-Al_2O_3 basal plane, **E** polarized perpendicular to the c axis.[11]

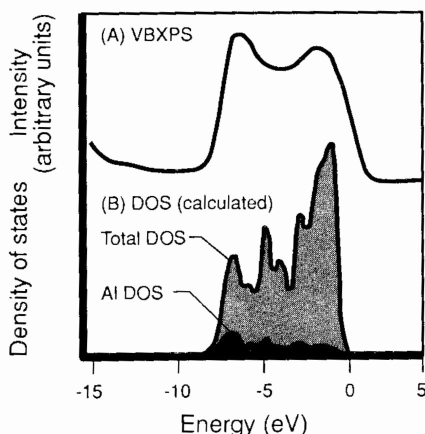

Fig. 4. Room-temperature VBXPS spectra of α-Al_2O_3 compared with the total and partial DOS calculated by the pseudofunction method.

gy. From absorption edge fitting, the absorption edge of Al_2O_3 is found to be exponential in nature, of the Urbach type,[30] seen for many ionic materials.[31] The **k**-space band diagram allows us to determine that the band gap of Al_2O_3 is direct at the Brillouin zone center, the Γ point.

The exciton peak at 9 eV in the reflectance (Fig. 1) corresponds to the formation of bound electron–hole pairs. The binding energy of the exciton, which is related to the dielectric constant of the material, determines the position of the exciton peak relative to the band gap energy. In alkali halides, the exciton binding energy can be on the order of 1 eV, whereas, in covalent materials, it can be on the order of 50 meV. In Al_2O_3 we expect the exciton binding energy to be low and the exciton to be nearly degenerate with the band gap. This conclusion is supported by recent work[32] on the exciton binding energy in MgO, which is 60 meV.

Let us consider the atomic origins[37] of the electronic bands of Al_2O_3. The top of the upper valence band arises from O $2p$ nonbonding orbitals. These bands are flat in **k** space and correspond to states which are localized in real space forming the familiar O^{2-} ion. The conduction bands arise predominantly from Al antibonding orbitals and are empty, corresponding to the formation of the Al^{3+} ion. The anionic character of the valence bands and the cationic character of the conduction bands of Al_2O_3 demonstrate the ionic nature of the bonding. In a covalent material such as GaAs, hybridization occurs in the bonding, and the valence and conduction bands each arise from mixed Ga and As orbitals or from hybridized "anion" and "cation" orbitals. From Pauling's electronegativity we know that Al_2O_3 is only partially ionic and the hybridization of Al and O states can be seen in the upper valence band, as shown by the partial atomic DOS determined by the PSF calculation. Below the O $2p$ nonbonding bands, are bands of mixed Al and O origin, and these hybridized Al–O bonding orbitals represent the covalent bonding present in Al_2O_3. The bottom of the conduction band states arises from delocalized Al $3s$ antibonding states. Higher up in the conduction bands we can see relatively flat bands which are Al $3p$ antibonding orbitals. The band gap of Al_2O_3 arises from O $2p$ to Al $3s$ transitions. Peak 1 in the reflectivity (Fig. 1) is excitonic in nature and associated with O $2p$ to Al $3s$ transitions, whereas peak 2 arises from O $2p$ to Al $3p$ transitions.

The band effective masses of valence and conduction band carriers can affect the mobility of free carriers and are determined by the band curvature in **k** space. The O $2p$ bands are very flat and have large band effective masses; the holes are heavy. The Al $3s$ bands are more free-electron-like, leading to small effective masses, whereas the Al $3p$ states give rise to larger effective masses. For an idea of the magnitudes of the band effective masses in Al_2O_3, we can consider results calculated for MgO (Ref. 32), where the band effective masses are $m^*_{h_1} = 1.35m_e$ and $m^*_{h_2} = 0.17m_e$ and $m^*_e = 0.14m_e$. The band effective masses should not be confused with the distinct effects of the lattice stabilization associated with polaron formation. Polaron formation can also lead to dramatic decreases in the carrier mobilities relative to free electron mobilities. The lattice relaxation associated with polaron formation involves both electronic charge and nuclear relaxations which require the electron–phonon interaction and is therefore outside the framework of the Born–Oppenheimer approximation used for band structure calculations. Still there is a correlation between the band widths and the formation of large and small polarons, because one electron bandwidths can be considered as a simple demonstration of real-space charge localization. For Al_2O_3 the valence and conduction band widths are such that we expect both electrons and holes to form large polarons. Materials which exhibit small polaron holes, with their associated thermally activated hopping mobility, have much narrower O $2p$ bands.

IV. High-Temperature Electronic Structure and Conductivity

The effects of temperature on the electronic structure of Al_2O_3 are important because of the mixed electronic–ionic character of its defect chemistry and the high-temperature processing and applications of Al_2O_3. The Born–Oppenheimer approximation[42,43] states that atoms can be considered to be frozen in the time scale of the electrons, and, therefore, we can study the electronic structure without reference to the effects of atomic motion or vibration as embodied in the electron–phonon interaction. This approximation is well satisfied at room temperature, but it is exactly the violation of the Born–Oppenheimer approximation which produces the large temperature dependences of the electronic structure which are essential for understanding the high-temperature behavior of Al_2O_3. At high temperatures, not only is there a temperature-dependent increase in the thermal carrier concentration, but also the electron–phonon interaction and thermal lattice expansion leads to a dramatic decrease in the band gap energy, with concomitant increases in the electronic carrier concentrations.

Upon heating a sample of Al_2O_3 from room temperature to 1573 K (Fig. 6), the absorption edge and reflectivity peaks shift to lower energies with increasing temperature. This is a direct measurement of the temperature dependence of the electronic structure.[4,44] We can fit the temperature dependence of the band gap with an equation of the form

$$E_g(T) = E_g(T=0\ K) + \beta T + \gamma T^2$$

where β is the linear and γ the quadratic temperature coefficient of the band gap. For α-Al_2O_3, the band gap shifts linearly; γ, the quadratic temperature coefficient, is negligable. The shift of the absorption edge seen in reflectance (Fig. 7) demonstrates that the band gap decreases linearly at a rate of −1.1 meV/K, which is much larger than that observed in the covalent semiconductors such as Si or Ge (−0.22 and −0.44 meV/K).[45] The exciton peak (peak 1) is also seen to shift to lower energies at −1.0 meV/K and to broaden and decrease in magnitude, because of phonon scattering of the excitonic electron-hole pairs. Peak 2, arising from a higher-lying interband transition, decreases more slowly at −0.7 meV/K. This temperature dependence of the electronic structure leads to a decrease in the optical band gap energy from 8.8 eV at 300 K to 7.2 eV at 1763 K.

The major contributions to the temperature dependence of the electronic structure of Al_2O_3 are thermal lattice expansion and the electron–phonon interaction.[44,46] The effects of thermal lattice expansion can be modeled as a hydrostatic dilatation of the room-temperature unit cell. Calculations of this sort, for thermal lattice expansion between room temperature and 1763 K, determine the hydrostatic deformation potential of the band gap to be 350 meV/(lin% strain) and demonstrate that thermal lattice expansion is responsible for −0.31 meV/K of the band gap temperature dependence. We have modeled the effects of the electron–phonon interaction using distorted lattice calculations for two different phonon modes, or lattice vibrations. We assumed that, at 1763 K, the amplitude of each phonon mode is 0.0135 nm (0.135 Å) for Al and 0.0107 nm (0.107 Å) for O, as given by the Debye–Waller factors determined from high-temperature X-ray and neutron diffraction.[47,48] The band structure of a distorted unit cell incorporating the frozen displacements of either an *a–b* plane or a *c* axis, symmetry-conserving phonon mode was calculated. These phonon modes contribute −0.62 meV/K to the band gap temperature dependence. The combined effects of lattice expansion and electron–phonon interaction are calculated to be −0.93 meV/K compared with their measured value of −1.1 meV/K as shown in Fig. 7. Only 33% of the band gap temperature dependence arises because of thermal lattice expansion, whereas the electron–phonon interaction plays the major role. Because of the complexity of the band structure calculations, these are the only phonon modes we have studied for Al_2O_3. A more comprehensive electron–phonon calculation would incorporate the manifold of possible phonon displacements and assign to each mode an amplitude appropriate to the energy and character of that mode in the phonon structure. We have performed more extensive theoretical calculations of the temperature dependence of the electronic structure in MgO covering 10 phonon modes, with (111), (100), and (110) displacements of different amplitudes and determined individual electron–phonon couplings.[32] The electron–phonon quasi particles, which show the strongest coupling, correspond to phonon modes in which the phonon displacements are normal to the nearest-neighbor bond lengths, thereby producing only small decreases in the Mg–O bond lengths.

The valence and conduction bands respond very differently to increasing temperature. Upon heating Al_2O_3 in situ during a VBXPS measurement, we observe no change in the valence band width (Fig. 8) within the resolution of the measurement. Calculations predict that lattice expansion narrows the upper valence band, which is at the same time counteracted by the electron–phonon-induced broadening of the band. The only apparent change in the valence bands is a slight

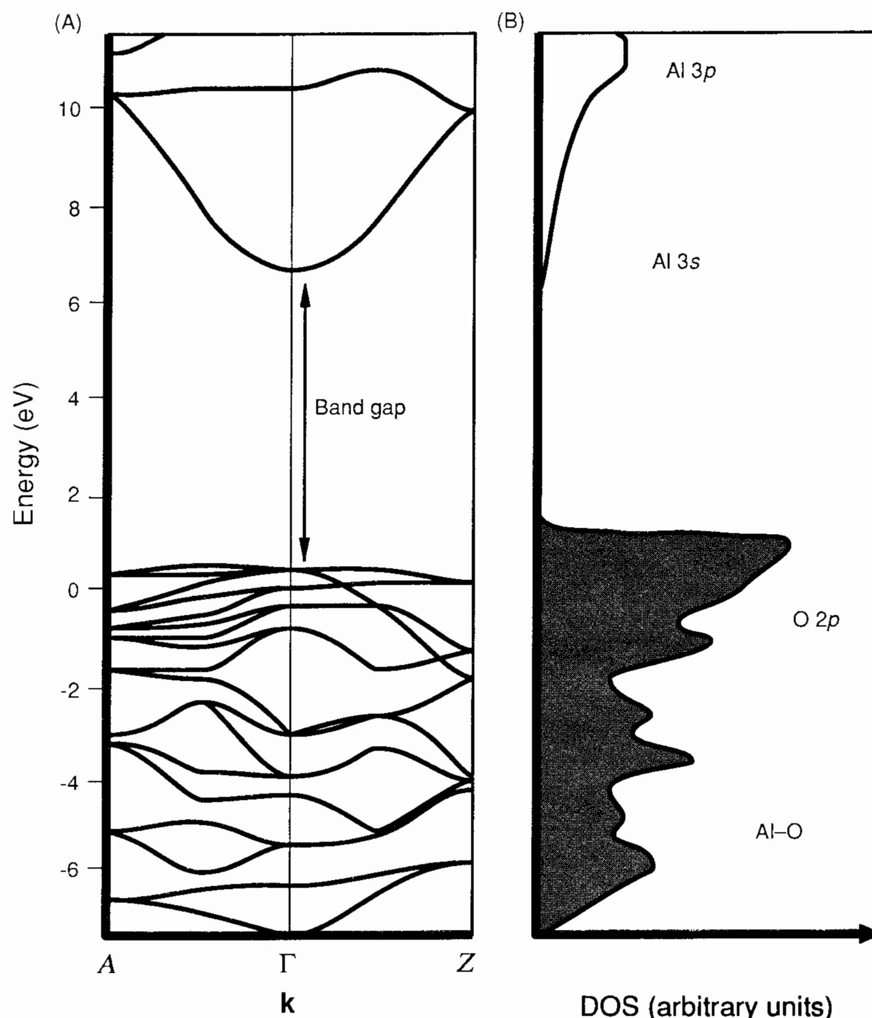

Fig. 5. (A) **k**-space energy bands and (B) total DOS for Al_2O_3 at room temperature as determined by pseudofunction band structure calculations.

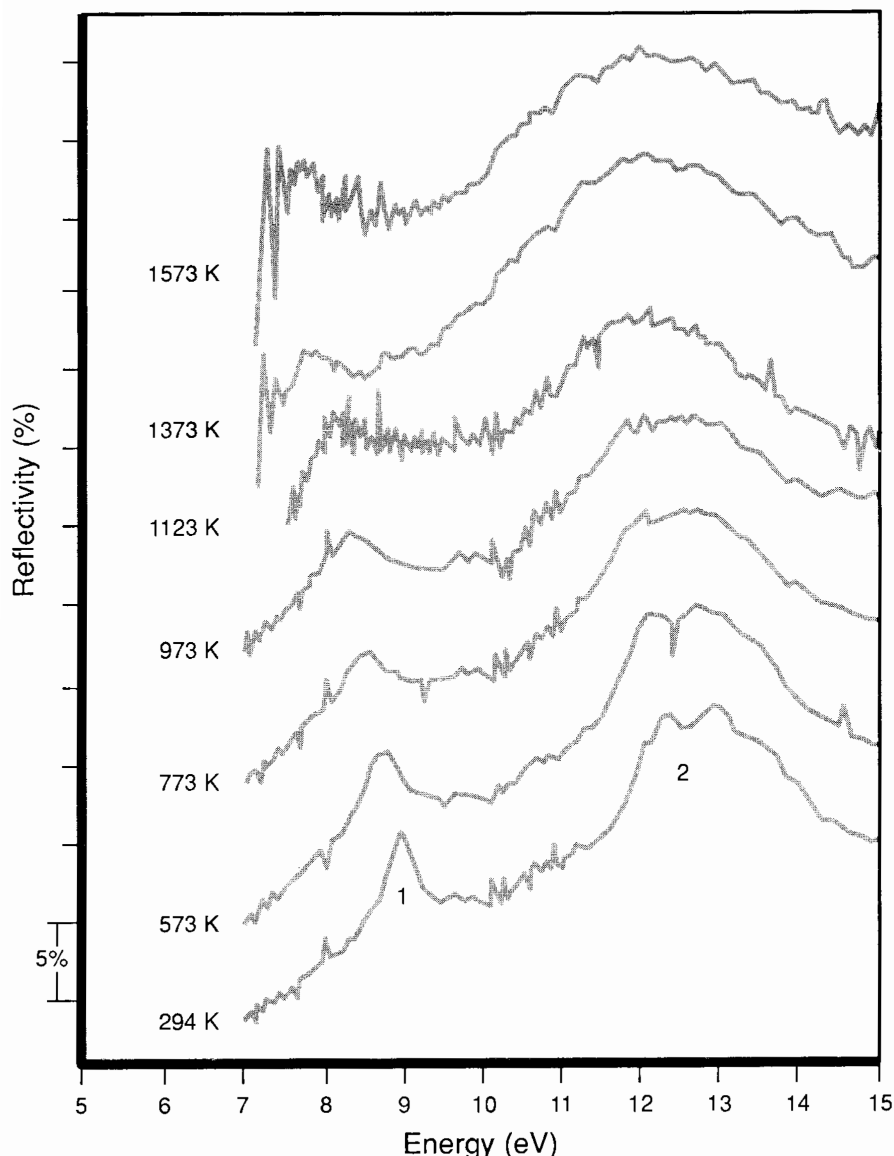

Fig. 6. Temperature-dependent VUV reflectance of single-crystal Al_2O_3 for **E** polarized parallel to the c axis.

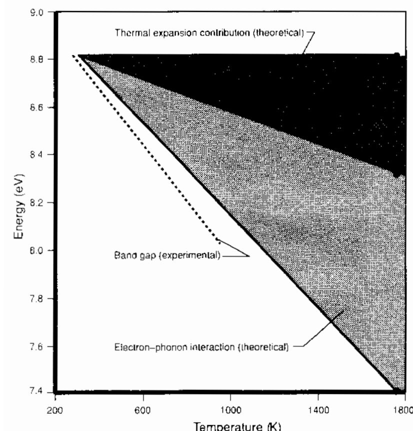

Fig. 7. Theoretically determined contributions of lattice expansion and the electron–phonon interaction to the temperature dependence of the band gap of α-Al_2O_3 (cross hatched) compared with the experimentally determined temperature dependence of the band gap.

increase in the separation of the O $2p$ and Al–O hybridized peak in the valence band. From the temperature coefficients of the various reflectivity features (Fig. 9), transitions to Al $3s$ bands shift at -1.1 meV/K, whereas transitions to the Al $3p$ bands shift at -0.7 meV/K with peak 2 also broadening. The band gap energy decreases noticeably, which may correspond to a shifting of the Al $3s$ bands down toward the valence bands. The smaller temperature dependence of peak 2 suggests that the Al $3p$ conduction bands are shifting at a reduced rate. More detailed critical point analysis, as has been done for MgO (Ref. 4), will give us more insight into the individual temperature-induced band shifts.

Our knowledge of the high-temperature electronic structure can be used to evaluate previous high-temperature conductivity experiments and also to suggest the use of this knowledge as a test of conductivity data.[49] In a high-temperature electronic conductivity measurement, transference number measurements can be used to separate ionic from electronic conductivity, and, by varying the partial pressure of oxygen, the electronic conductivity can be varied from electronic (donor-dominated) to hole (acceptor-dominated) conductivity. The intermediate point where $\sigma_e = \sigma_h$ is defined as the intrinsic point and serves as a probe of the intrinsic conductivity of the material, unaffected by carriers arising from extrinsic sources, such as impurities or dopants. The intrinsic point conductivity of α-Al_2O_3 can be calculated from Eq. (1), which has been developed based on the fundamental, intrinsic material parameters of α-Al_2O_3 and assumed large polarons as the charge carriers.

$$\frac{\sigma_e \sigma_h}{T^2} = 163\left(\frac{m_e^* m_h^*}{m_e m_e}\right)^{1/2} \times f(\alpha_e)\, f(\alpha_h)\, \exp(\beta/k) \times \exp[(-E_g^\circ - \Delta)/kT] \quad (1)$$

where $f(\alpha) \approx 0.2$ for $\alpha = 2.7$, where

$$f(\alpha) = \left[\frac{1 - 0.0008\alpha^2)\alpha}{1 - (1/6)\alpha + 0.0034\alpha^2}\right]^{-1}$$

The intrinsic point conductivity depends on the band effective masses m_e^* and m_h^*, the polaron-coupling constant α (which determines the polaron effective mass), the band gap temperature dependence β (1.1 meV/K), the optical band gap energy E_g° ($T = 0$ K) (9.1 eV), and the lattice stabilization energy or Stokes shift Δ (associated with the thermal band gap energy for polaron formation). The temperature dependence of the band gap, β, plays a major role in the high-temperature electronic conductivity: $\exp(\beta/k)$ is a factor of 10^5 for Al_2O_3. The slope of the intrinsic-point conductivity, plotted as $\sigma_e\sigma_h/T^2$ vs $1/T$, can be used to determine the $T = 0$ K thermal band gap energy. The thermal band gap of Al_2O_3 will be reduced from this optical value by the lattice stabilization energy of the polarons. This Stokes shift is at present not known, but it appears reasonable that the Stokes shift is on the order of 1 eV. We therefore have a strong test of conductivity data: the intrinsic-point slope must be less than 9.1 eV to be consistent with our knowledge of the electronic structure of Al_2O_3. In addition, using estimates of carrier mobilities, we can calculate the magnitude of the intrinsic-point conductivity at high temperature. Evaluating the data of Kroger[50,51] and Kitazawa[52] in this manner, we find that Kroger's result for the magnitude of the intrinsic electronic conductivity is too low, while the slope of his intrinsic-point conductivity is too large. Kitazawa's data are consistent with the

high-temperature electronic structure discussed here. This supports Kitazawa's finding that Al_2O_3 is predominantly an electronic conductor at high temperatures. The high-temperature electronic structure, determined by spectroscopic and theoretical techniques, independent of conductivity measurements, can provide a strong test of the validity of high-temperature conductivity data. We hope that the existence of this test will promote the application of conductivity techniques to the challenging problem of the high-temperature defect chemistry of Al_2O_3.

V. Deformation Potentials and Surface Stress Determination

Ruby *R*-line fluorescence[53,54] is an optical method of determining bulk stress in Al_2O_3 which is the basis of pressure measurement used in diamond anvil cell studies.[55] In this case, pressure causes a continuous shift of the orbital energies of the Cr^{3+} ion, and the shift of the red fluorescence emission of Cr is used with calibration coefficients to measure the stress. This is a bulk measurement of stress because the *R*-line signal originates throughout the bulk of the sample, Al_2O_3 being transparent in the visible. In a similar way a surface sensitive probe of stress[56] is possible using VUV measurements at the band gap energy, where Al_2O_3 is strongly absorbing, once the deformation potentials of the band gap are known. The hydrostatic dilatation of the lattice arising from thermal lattice expansion, which contributes to the temperature dependence of the band gap, is analogous to stress in hydrostatic dilatation. Therefore, from calculations of the effect of thermal lattice expansion on the band gap energy, we also determine the hydrostatic deformation potential of the band gap, which for Al_2O_3 is 350 meV/(lin% strain). Using VUV reflectivity measurements we can determine the exciton peak position at room temperature from the surface of a sample of single-crystal or polycrystalline Al_2O_3. Figure 10 shows the changes in the exciton peak position for samples which have been mechanically polished with 1-μm diamond paste or chem-mechanically polished with colloidal silica. The exciton peak shifts 0.26 eV to higher energy in the diamond-polished samples. This polishing-induced peak shift can be observed in either single-crystal or polycrystalline Al_2O_3 and is only dependent on the polishing-induced surface damage. The VUV light probes a surface layer of the material, determined by the absorption coefficient at the band gap energy, which for the exciton in Al_2O_3 is on the order of 0.05 to 0.5 μm deep. This

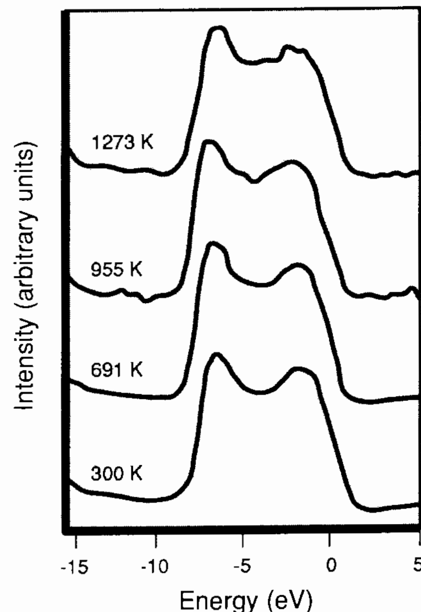

Fig. 8. Temperature-dependent VBXPS of α-Al_2O_3 as a function of temperature.

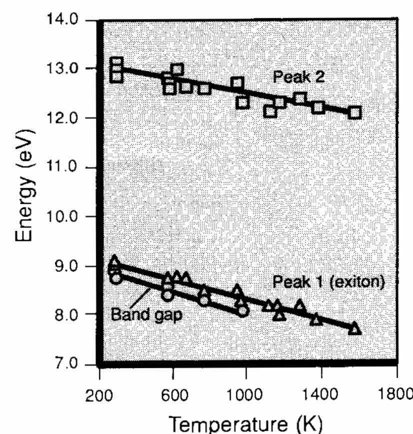

Fig. 9. Temperature-dependent transition energies of the band gap (O 2*p* to Al 3*s*), peak 1 (exciton), and peak 2 (O 2*p* to Al 3*p*) of single-crystal α-Al_2O_3.

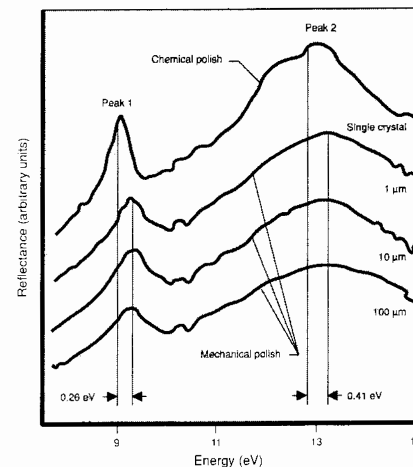

Fig. 10. VUV reflectivity of chemically polished single-crystal α-Al_2O_3 basal plane compared with mechanically polished polycrystalline α-Al_2O_3.[56]

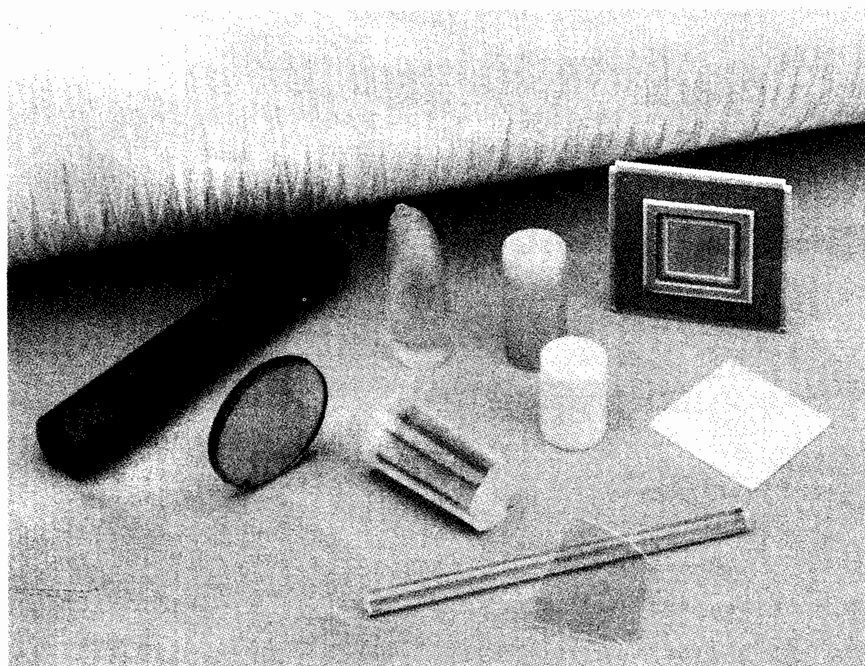

Al_2O_3 has a wide variety of technological applications as a structural, electronic, and optical material. In this photo are shown samples of single-crystal and polycrystalline Al_2O_3. Cr-doped α-Al_2O_3 is used as the lasing medium in ruby lasers and Ti-doped α-Al_2O_3 has recently developed as a new tunable laser material. Undoped α-Al_2O_3 is used as an optical window material and as a substrate for epitaxial growth of Si on sapphire for electronic device fabrication. Translucent polycrystalline α-Al_2O_3 such as this Lucalox (registered trademark of General Electric Company, Schenectady, NY) is used as an optical and structural material in Na-vapor arc lamps. Polycrystalline α-Al_2O_3 is used as a structural and high-temperature refractory material and is also the basis of high-temperature cofired electronic packages for integrated circuits and microelectronic hybrid device fabrication. Continuous filament α-Al_2O_3 fibers such as Fiber-FP (registered E. I. du Pont de Nemours & Co., Inc.) plays an important part in many new metal matrix and ceramic matrix composite applications. A complete understanding of the electronic structure of Al_2O_3 can help guide developments in all of these areas.

is a very useful surface layer sensitivity and can be applied to measure polishing-induced surface layer stresses. The stress state in a layer damaged by polishing is biaxial, with the stresses in-plane and zero stress out-of-plane. This complex stress state, involving both hydrostatic and shear components, requires knowledge of both the hydrostatic and shear deformation potentials to accurately determine the magnitude of the stress. At present we do not have direct experimental measurements of both the hydrostatic and shear deformation potentials of the band gap, but upon their determination we will have a sensitive method to measure surface stresses.

VI. Al_2O_3 and AlN: Electronic Structure and Copper Bonding

We can gain insight into atomic bond formation at bimaterial interfaces by considering the bond formation at the atomic and the one-electron level.[57] At the same time, by contrasting the electronic structure of a predominantly ionic ceramic such as Al_2O_3 with a more covalent material such as AlN, we can understand

Band Structure Calculations

The energy levels of carbon atoms as they are brought from infinity to form diamond demonstrates the evolution of energy bands.[24,25] As the orbitals or electron wavefunctions overlap, they must broaden out, forming energy bands because of the Pauli exclusion principle. The band gap energy is defined as the energy between the filled valence bands and the unoccupied conduction bands

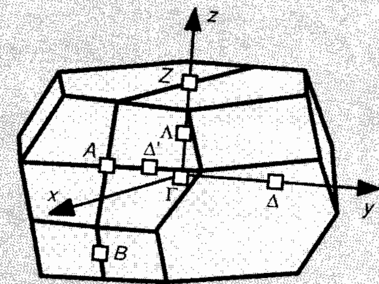

The reciprocal space Brillouin zone of the real-space hexagonal unit cell of α-Al_2O_3.

Band structure calculations of the energy bands are performed using the fundamental unit cell and the long-range periodicity of the crystal. The electron wavefunctions must satisfy Schroedinger's wave equation and, because of the periodicity of the crystal, will assume the form of Bloch waves.[26] The band structure calculation of the electron wavefunctions (eigenfunctions) and energies (eigenvectors) of Schroedinger's equation for the crystal is conducted in reciprocal or **k** space, where **k**, the reciprocal lattice vector, equals $2\pi/\mathbf{a}$, **a** being the real-space lattice vector. The magnitude of **k** is related to the momentum of the electron. The real-space unit cell of the crystal is transformed into reciprocal space producing the Brillouin zone (BZ)[27] of the band structure calculation. Each crystalline unit cell has various symmetry properties; embodied in it are space and point groups, and this symmetry is also present in the BZ. The BZ for Al_2O_3 is shown here and Γ is defined as the center of the BZ where $\mathbf{k} = 0$, while A, B, Z, and Λ are other high-symmetry locations. The band structure diagram represents the energies of each of the calculated bands at various high-symmetry points in **k** space. The symmetry of each electron wavefunction determines the orbital character of the band and dictates which bands will be degenerate (have the same energy) at certain places in the BZ, and when band splitting will occur along certain directions in the BZ. The wavefunction symmetries also determine whether the oscillator strength or matrix element for an optical transition will be large.

An interband transition is direct if it is vertical in the band structure diagram, leading to no change in the **k** vector or momentum of the electron. In an indirect interband transition, the momentum of the electron is changed, and the transition is not vertical in the band diagram. Because photons have negligible momentum, they can only excite direction transitions, unless there is the cooperation of a lattice phonon to change the momentum of the electron. The distinction between direct and indirect transitions gives rise to the identification of the band gap energies as direct and indirect band gap energies. These should not be confused with the very different distinction between optical and thermal band gaps. If we evaluate throughout the BZ the number of electron states present at one energy, ignoring their location in the BZ, we determine the DOS.

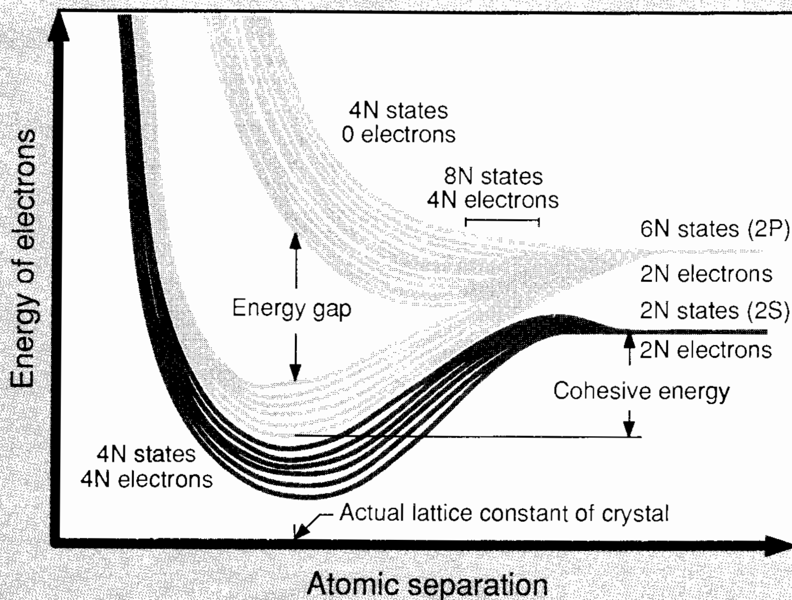

The development of the valence and conduction bands of diamond is shown as a function of atomic separation.

the role of covalency and the electronic structure in interfacial bond formation. Consider the evolution of the electronic structure of Al cation ceramics as we vary the anion from oxygen to nitrogen, with AlON as a useful intermediate material along this compositional line.[58] As we vary from Al_2O_3 to AlN, we are not forming a true solid solution because of the various intermediate phases and crystal structures (α-Al_2O_3, γ-Al_2O_3, and various AlON phases to AlN), but the variation in the valence bands is still illustrative of what can be called "valence band chemistry." The variation in the absorption coefficient at the band gap for thin films[59] of Al_2O_3, AlON, and AlN is shown in Fig. 11. The band gaps of AlN and AlON are 5.8 and 6.2 eV, respectively, with AlON exhibiting a smaller absorption edge slope. Upon removing all of the nitrogen, the band gap jumps dramatically up to 7.2 eV for the γ-Al_2O_3 thin film. The valence band DOS determined by VBXPS (Fig. 12) helps explain these changes in band gap. In AlN the top of the upper valence band is of N *2p* character with the Al–N hybridized levels in the bottom of the upper valence band. The nitrogen bands lie at higher energy than the O *2p* and Al–O bands in Al_2O_3. Therefore, in AlN, the valence bands lie closer to the Al conduction bands than in Al_2O_3, leading to a reduced

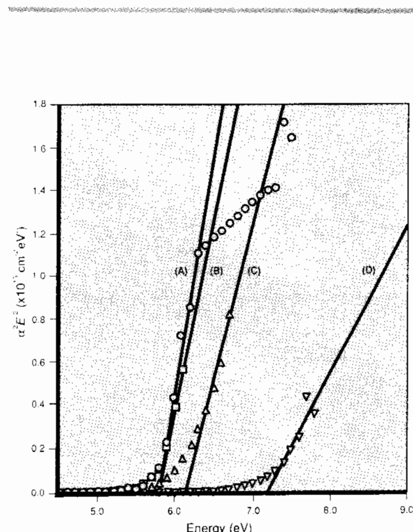

Fig. 11. Absorption coefficients plotted for direct absorption edge analysis of (A) AlN doped with 2% O (E_g = 5.8 eV), (B) AlN doped with 8% O (E_g = 5.8 eV), (C) AlON (E_g = 6.2 eV), and (D) γ-Al_2O_3 (E_g = 7.2 eV) thin films, and showing the changes in absorption edge shape and band gap energy with changing N to O ratio.[9]

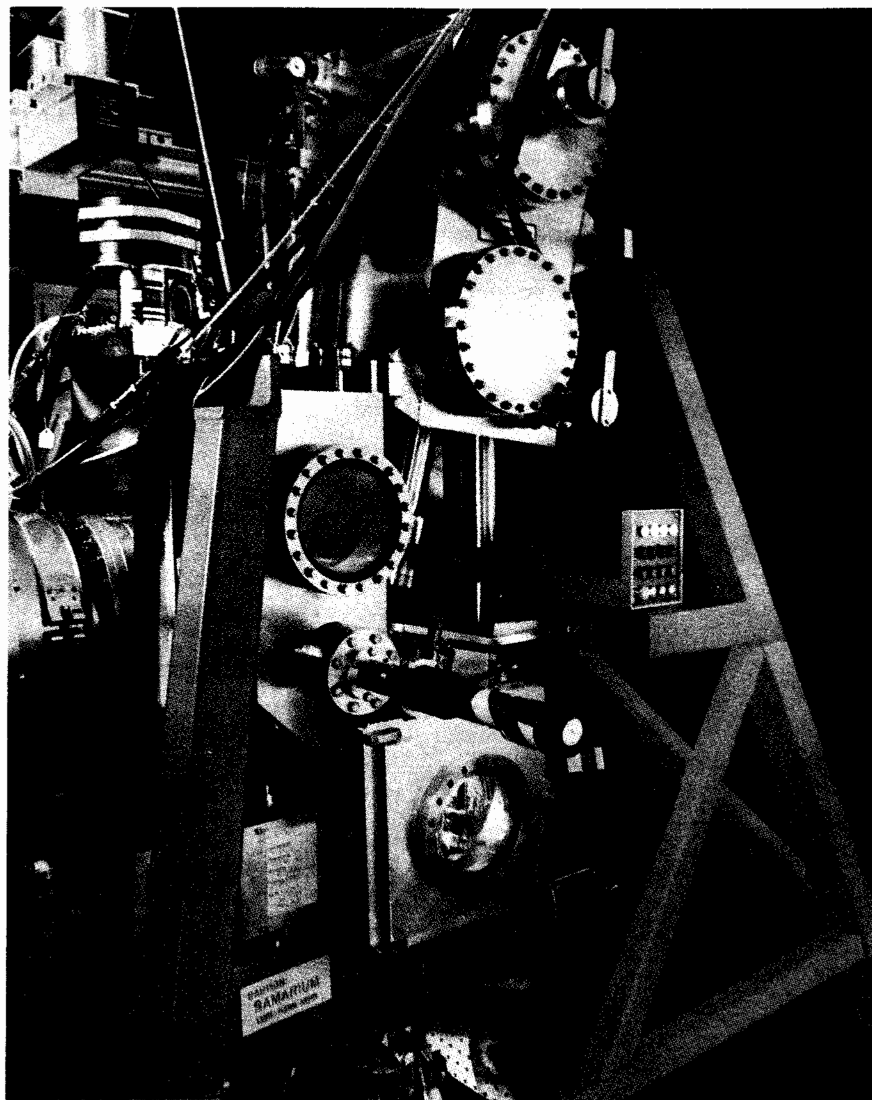

Shown is the LPLS VUV spectrophotometer which performs optical reflectance, transmission, fluorescence, and photoconductivity measurements. The energy range of the spectrophotometer is from 1.7 to 40 eV (700 to 31 nm), encompassing the visible, ultraviolet, and vacuum ultraviolet spectral regions. Measurements are taken with 0.1- and 0.3-nm resolution. The temperature of the sample can be varied from 10 K (using a He cryostat) to 2000 K (using CO_2 laser heating) to study the temperature dependence of the electronic structure and the effects of the electron–phonon interaction and thermal lattice expansion. The spectrophotometer uses dispersive analysis, the LPLS produces high brightness time resolved light of 10-ns duration, and polychromatic LPLS light is incident on the sample before entering the polychromator. The 1024-element photon counting detector is also time resolved, and acquires data in a complete spectral region simultaneously.

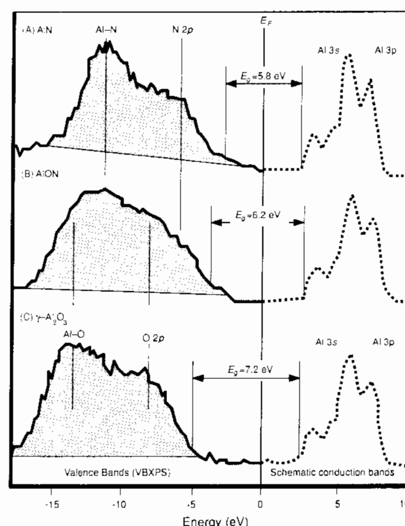

Fig. 12. Electronic structure of the AlN–AlON–γ-Al_2O_3 ceramics as the anion is changed from nitrogen to oxygen. The valence band DOS are determined from VBXPS measurements, whereas the conduction band DOS are a schematic representation of the Al *3s* and *3p* bands. (E_F is the Fermi energy.)

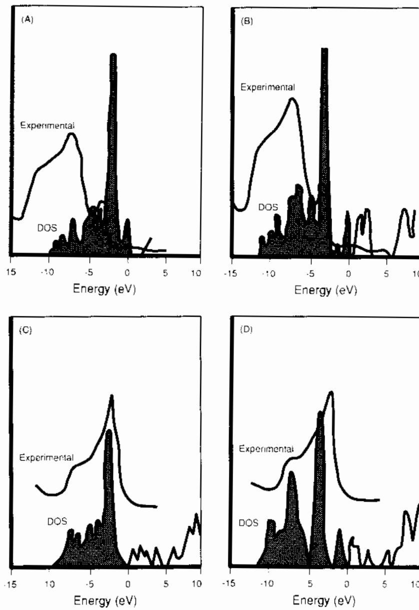

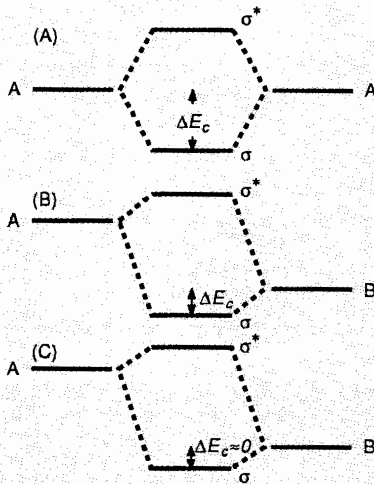

Fig. 13. Comparison of the experimentally measured and calculated DOS for Cu on Al_2O_3 (Ref. 62) and AlN (Ref. 61). Cu on Al_2O_3 with (A) Cu atom over the Al surface site, poor DOS agreement and (B) Cu atom over the O surface site, good DOS agreement for Cu 3*d* peak. Cu on AlN with (C) Cu atom over the Al surface site, good DOS agreement for Cu 3*d* peak, and (D) Cu atom over the N surface site, poor DOS agreement.

value of the band gap energy. Instead of having the two peaks in the upper valence band characteristic of both AlN and Al_2O_3, the AlON thin film has four components in the upper valence band arising respectively from N 2*p*, O 2*p*, Al–N, and Al–O. For the AlON thin film, the band gap is similar to AlN because the origin of the band gap transitions remains from N 2*p* to Al 3*s* bands, but the absorption edge slope and the number of valence-to-conduction band transitions is reduced in AlON, because of the removal of one-half of the N 2*p* states and their replacement with lower-lying O 2*p* states.

We have studied room-temperature bonding of monolayer coverages of Cu to thin films on Al_2O_3 and AlN using UPS and ab initio total-energy PSF calculations.[60–62] The differences in the occupied valence bands among these three materials lead to dramatic differences in the room-temperature bonding of Cu to these materials. Upon deposition of the first monolayer of Cu on Al_2O_3 or AlN, the Cu 3*d* level is seen shifted from its metallic position, in the middle of the band gap of the substrate, down toward the upper valence band. This reduction in the energy of the Cu 3*d* level is indicative of the bond stabilization associated with Cu-3*d*-to-ceramic bond formation. The decrease in the Cu 3*d* level is found to be greater on AlN than Al_2O_3, suggesting stronger chemical bond formation.

To understand the nature of this bond formation and to identify the atomic surface site at which the bonds form, we calculated the band structures for one-half monolayer coverage of Cu on Al_2O_3 and AlN. The Cu atoms in the calculations were placed over the cation (Al) or anion (oxygen in Al_2O_3 or nitrogen in AlN) surface atom. The surface structures of the Al_2O_3 and AlN were bulk-terminated structures, while the Cu-substrate bond lengths were allowed to vary in length, and the total energy of the system minimized to determine the equilibrium Cu-substrate bond length. The equilibrium Cu-substrate bond lengths were for Al_2O_3, a Cu–O bond length of 0.185 nm (1.85 Å) and a Cu–Al bond length of 0.255 nm (2.55 Å), whereas for AlN the Cu–N bond length was 0.19 nm (1.9 Å); the Cu–Al bond length was 0.26 nm (2.6 Å). For Cu on Al_2O_3 the total energy per surface Cu atom is 2.5 eV less (greater stability) for Cu–O bond formation than that for Cu–Al bond formation. For Cu on AlN, the total energy per surface Cu atom is 3.1 eV less for Cu–Al bond formation

Chemical Perspective on Bonding

Molecular orbital diagrams: (A) Covalent bond formation occurs between orbitals initially at the same energy. The covalency, represented by ΔE_c, is maximized. Note the σ bonding and σ^* antibonding orbitals. (B) Mixed ionic–covalent bond formation occurs when the orbitals are at different initial energies, representing an electronegativity difference between the orbitals. (C) Ionic bonding occurs when there is a large electronegativity and energy difference between the orbitals. Covalency is minimized and most of the bond stabilization arises from ionic stabilization.

A localized chemical perspective, such as molecular orbital or ligand field theory can supply useful insight into the electronic structure and the ionic or covalent nature of bond formation. In the diagram taken from Huheey[38] are shown the molecular orbital diagrams for covalent and ionic bond formation. Covalent bonds are characterized by mixing of the orbitals on each atom and sharing of electrons in the bonding orbital; the unoccupied higher orbital is of an antibonding character. Orbitals which are not involved in bond formation are referred to as nonbonding orbitals, such as the O 2*p* lone pairs which form the top of the valence band in Al_2O_3. The degree of ionicity of the bond is determined from the electronegativity difference between the two atoms, and it appears as the initial energy difference between the two orbitals forming the bond. The bond formation diagram is for the case of HCl, where, during the process, sp^3 hybridization of the Cl orbitals occurs, maximizing the covalency of this bond.

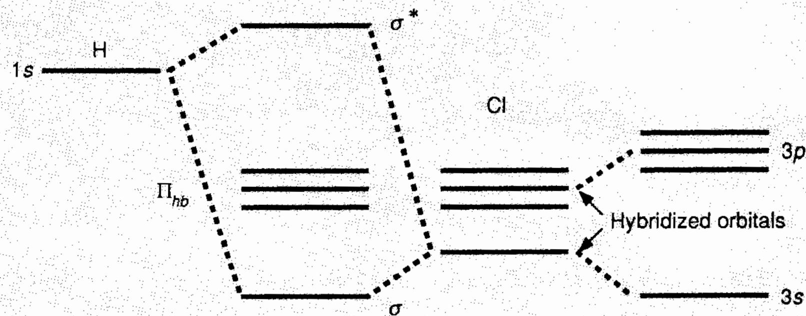

Bond of H to Cl demonstrates the hybridization of the Cl *s* and *p* orbitals. Three orbitals of Cl are unable to participate in bond formation and form nonbonding orbitals in the molecule.

than for Cu–N bond formation. In Fig. 13 the calculated total DOS of the slab for each bonding surface site is shown and compared with the experimentally determined DOS. The DOS in Fig. 13 is shown referenced to the theoretical Fermi energy, whereby occupied states are below 0 eV, whereas states above 0 eV are unoccupied. The experimental UPS DOS did not have an absolute binding energy reference. For Al_2O_3, the experimentally observed peak in the DOS arising from the narrow Cu 3*d* level agrees with the calculated DOS only for Cu atoms which are situated over the oxygen site, the minimum total-energy configuration. Cu bonds to Al_2O_3 by an ionic process, where there is charge transfer between the Cu and O atoms followed by electrostatic attraction of the ionic species. For the case of Cu on AlN, the bonding is of a very different character. For the covalent substrate material, agreement is found in the DOS and total-energy results only for siting of the Cu atom over the Al atoms on the surface of AlN. This would correspond to an electron-sharing type of bond formation more typical of metallic or covalent bonding, and this bond exhibits greater stabilization and is stronger. The formation of a metallic Cu–Al bond is also supported by observing the Al 2*s* core level spectra which, with increasing Cu coverage, splits into two components.

Cu–Al_2O_3 and Cu–AlN, respectively, are two examples of bonding to an ionic and a covalent ceramic and show different types of bond formation with different atomic sites and bond strengths. For AlN ceramics processed in air, the bond formation will be different than that observed under UHV conditions because there will be an oxidized surface layer present, and, therefore, the bonding will be of the ionic nature of Cu–Al_2O_3. Insight into the electronic nature of bonding at biomaterial interfaces can give us a useful way to understand the wide variety of phenomena occurring at bimaterial interfaces.

VII. Conclusions

The past years have seen a new focus on the electronic structure of ceramic materials. Advances in spectroscopic techniques and theoretical methods have increased our understanding of the role of the band structure in determining the properties of Al_2O_3 at high temperature, under stress, the effects of compositional variation, and the electronic nature of bond formation at interfaces. The electronic structure of Al_2O_3 at high temperature is controlled by the effects of thermal lattice expansion and the electron–phonon interaction. These cause shifts and broadening of the valence and conduction bands, leading to dramatic increases in the electronic carrier concentrations. The strain dependence of the electronic structure, as embodied in the deformation potentials, produces a simple method for measuring surface strains and stresses in Al_2O_3.

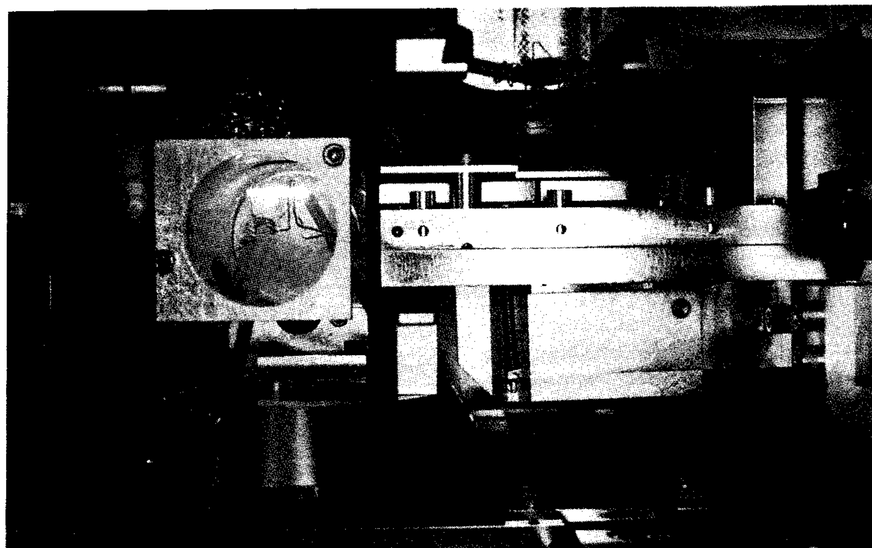

A sample of single crystal α-Al_2O_3 mounted on a sapphire tripod stand in the laser plasma light sourced, vacuum ultraviolet spectrophotometer. The sample is heated to 2000 K by a 150-W CO_2 laser for high-energy, high-temperature VUV reflectance measurements to measure the high temperature electronic structure. The use of CO_2 laser heating avoids the problems of impurity deposition and contamination of the sample surface which can arise in conventional furnace heating. To the upper right of the reflectance sample is shown a ruby crystal mounted on the transmission sample holder (which can also be laser heated). Above the sample the helium cryostat used for low temperature (10 to 450 K) measurements can be seen. The light from the Sm laser plasma light source descends from the upper left, reflects off of the sample, and enters the slit of the polychromator to the upper right. The light is then incident on the 1024-element multichannel detector of this dispersive analysis optical spectrophotometer.

Excitons

Upon excitation of an electron into the Al conduction band, a positively charged hole is left in the top of the valence band, residing on the adjacent O atom. An exciton is formed when the electrostatic attraction between this electron and hole is sufficient to create a bound electron-hole pair.[33,34] The size of the excitonic particle varies with the ionicity or covalency of the material. Excitons in semiconductors can have sizes of tens of nanometers (hundreds of Ångstroms), whereas, in ionic solids they may be only 0.5 or 1.0 nm (5 or 10 Å) in size. The exciton can be considered analogous to the H atom; it exhibits a similar series of excited states, and the binding energy $E_{BE}^{exciton}$ is determined by the electrostatic attraction of the electron and the hole. In the ground state of the exciton, it will appear in the optical spectrum at an energy of $E_g^{optical} - E_{BE}^{exciton}$ and can exhibit excited states up to a value of $E_g^{optical}$, corresponding to the excited state with index $n=\infty$, at which point it will be ionized and the electron and hole will dissociate.

Excitons can serve as useful probes in materials because they are localized particles of neutral charge. Line shape analysis[35,36] of the exciton peak can be used to probe the scattering of excitons by phonons or defects, giving insight into defect densities, damage, exciton–phonon coupling, and the effects of temperature. A Lorentzian exciton peak is representative of weak exciton scattering and is observed in cleaved crystals of MgO at or below room temperature.[4] In Al_2O_3, even at low temperatures, the exciton peak shape is Gaussian, demonstrating strong exciton scattering, due to the defect density present in the surface of cut and polished samples of Al_2O_3.

The variation in the electronic structure upon replacement of the oxygen anion with nitrogen, an example of valence band chemistry, highlights the importance of ionicity and covalency in the electronic structure and in determining the properties of ceramics. The atomistic and electronic nature of metal–ceramic bonding at interfaces changes dramatically between ionic and covalent materials and gives us new insight about how dissimilar materials interact in complex multicomponent and multiphase materials. The studies to date serve as a first view of the electronic structure of a ceramic; future work and more detailed analysis will more fully elucidate the fundamental role of the electronic structure of ceramic materials.

Effective Masses of Electrons and Polarons

The mass of a conduction band electron, referred to as the band effective mass (m^*_{band}), can be modified from the rest mass of an electron in free space (m_e) by the diffraction effects of the crystal on the motion of the electron. The band effective mass can be calculated[39] from the curvature of the band in **k** space as follows:

$$m^*_{band} = \left(\frac{1}{\hbar^2}\frac{d^2E}{d\mathbf{k}^2}\right)^{-1}$$

where $\hbar$ is Planck's constant divided by 2π and **k** is the reciprocal lattice vector. In a material such as Al_2O_3, conduction band electrons form large polarons which behave as band carriers with an additional increase in effective mass due to the additional work required to overcome the effects of the associated lattice polarization field or phonon cloud. The strength of the electron–phonon interaction between the band electron and the lattice is given by the polaron-coupling constant α, and it determines the increase in the band effective mass due to polaron formation. α has been calculated to be 2.7 for Al_2O_3.[40] The polaron effective mass is given by the following equation:[41]

$$m^*_{polaron} = m^*_{band}\left(\frac{1-0.008\alpha^2}{1-(1/6)\alpha+0.0034\alpha^2}\right)$$

The case for the effective masses of holes is analogous to the electron case. Therefore, there are two major contributions to the effective mass of the polaronic charge carriers of Al_2O_3: first the band structure of Al_2O_3 modifies the rest mass of the electron to m^*_{band}, and second the electron–phonon interaction determines the polaronic carrier mass $m^*_{polaron}$.

Acknowledgments: The author acknowledges the essential contributions of F. S. Ohuchi for photoemission spectroscopy of ceramics, and R. V. Kasowski for pseudofunction band structure calculations. It is the combined power of this multidisciplinary work which has produced such a comprehensive understanding of the band structure of Al_2O_3. The assistance of D. J. Jones, M. L. Bortz, H. Song, M. E. Innocenzi, H. P. Jenssen, and R. D. Fancy (Acton Research Corporation) in VUV spectroscopy has been of great importance in addressing many of these topics. The assistance of M. L. Bortz, D. J. Jones, and G. W. Scherer in the preparation of this manuscript is appreciated. The guidance and support of R. L. Coble in highlighting the importance of the electronic structure of ceramics was instrumental.

References

[1] I. P. Batra, "Electronic Structure of α-Al_2O_3," *J. Phys. C: Solid State Phys.*, **15**, 5399–410 (1982).

[2] S. Ciraci and I. P. Batra, "Electronic Structure of α-Al_2O_3 and its Defect States," *Phys. Rev. B: Condens. Matter*, **28** [2] 982 (1983).

[3] X. Shangda, G. Changxin, L. Libin, and D. E. Ellis, "Electronic Structure of Alumina and Ruby," *Phys. Rev. B: Condens. Matter*, **35**, 9311 (1987).

[4] M. L. Bortz, R. H. French, D. J. Jones, R. V. Kasowski, and F. S. Ohuchi, "Temperature Dependence of the Electronic Structure of Al_2O_3, $MgAl_2O_4$, and MgO"; in Proceedings of the Ninth International Vacuum Ultraviolet Radiation Physics Conference, Hawaii, to be published in *Phys. Scr.*, **41** [4] (1990).

[5] R. Wooten, Optical Properties of Solids. Academic Press, New York, 1972.

[6] Handbook of Optical Constants of Solids. Edited by E. D. Palik. Academic Press, New York, 1985.

[7] J. I. Pankove, Optical Processes in Semiconductors. Dover, New York, 1971.

[8] Y. Petroff, "Optical Properties of Semiconductors above the Band Edge"; pp. 1–45 in Handbook on Semiconductors, Vol. 2, Optical Properties of Solids. Edited by M. Balkanski. North-Holland, New York, 1980.

[9] R. H. French, "Vacuum Ultraviolet Spectroscopy of Ceramics"; pp. 406–14 in Ceramic Transactions, Vol. 5, Advanced Characterization Techniques for Ceramics. Edited by W. S. Young, G. L. McKay, and G. E. Pike. American Ceramic Society, Westerville, OH, 1989.

[10] J. A. R. Samson, Techniques of Vacuum Ultraviolet Spectroscopy. Pied Publications, Lincoln, NE, 1967.

[11] M. L. Bortz and R. H. French, "Optical Reflectivity Measurements Using a Laser Plasma Light Source," *Appl. Phys. Lett.*, **55** [19] 1955–57 (1989).

[12] R. H. French, "Laser-Plasma Sourced, Temperature-Dependent VUV Spectrophotometer Using Dispersive Analysis"; in Proceedings of the Ninth International Vacuum Ultraviolet Radiation Physics Conference, Hawaii, to be published in *Phys. Scr.*, **41** [4] 1990.

[13] M. L. Bortz and R. H. French, "Quantitative, FFT-Based, Kramers–Kronig Analysis for Reflectance Data," *Appl. Spectrosc.*, **43** [8] 1498 (1989).

[14] J. Appel, "Polarons" (Edited by F. Seitz, D. Turnbull, and H. Ehrenreich), *Solid State Phys.*, **21**, 193–391 (1968).

[15] Polarons and Excitons. Edited by C. G. Kuper and G. D. Whitfield. Plenum Press, New York, 1962.

[16] M. E. Innocenzi, R. T. Swimm, M. Bass, R. H. French, A. B. Villaverde, and M. R. Kokta, "Room-Temperature Optical Absorption in Undoped α-Al_2O_3"; to be published in *J. Appl. Phys.*

[17] P. Lautenschlager, M. Garriga, L. Vina, and M. Cardona, "Temperature Dependence of the Dielectric Function and Interband Critical Points in Silicon," *Phys. Rev. B: Condens. Matter*, **36** [9] 4821–30 (1987).

[18] D. Y. Smith, "Dispersion Theory, Sum Rules, and Their Application to the Analysis of Optical Data"; pp. 35–68 in Handbook of Optical Constants of Solids. Edited by E. D. Palik. Academic Press, New York, 1985.

[19] G. Margaritondo and J. H. Weaver, "Photoemission Spectroscopy of Valence States"; pp. 127–85 in Methods of Experimental Physics, Vol. 22. Edited by R. L. Park and M. G. Lagally. Academic Press, New York, 1985.

[20] R. V. Kasowski, T. N. Rhodin, M. H. Tsai, and D. D. Chamblis, "Pseudofunction Method: Application to a Monolayer of CO and to the Si (100) Surface," *Phys. Rev. B: Condens. Matter*, **34**, 2656–59 (1986).

[21] R. V. Kasowski, T. N. Rhodin, and M. H. Tsai, "Chemisorptive Bonding of Carbon Monoxide on Ni (001), Formulations and Application of a New Pseudofunctional Electron Muffin Tin Approach," *Appl. Phys. A.*, **41**, 61–73 (1986).

[22] R. V. Kasowski, M. H. Tsai, and T. N. Rhodin, "Structural and Electronic Properties of CO Monolayer," *Solid State Commun.*, **59**, 57–60 (1986).

[23] R. Car and M. Parrinello, "Unified Approach for Molecular Dynamics and Density-Functional Theory," *Phys. Rev. Lett.*, **55** [22] 2471–74 (1985).

[24] J. I. Pankove, Optical Processes in Semiconductors; p. 2. Dover, New York, 1971.

[25] G. E. Kimball, "The Electronic Structure of Diamond," *J. Chem. Phys.*, **3**, 560–64 (1935).

[26] C. Kittel, Solid State Physics; p. 183. Wiley, New York, 1976.

[27] L. P. Bouckaert, R. Smoluchowski, and E. Wigner, "Theory of Brillouin Zones and Symmetry Properties of Wave Function in Crystals," *Phys. Rev.*, **50**, 58–67 (1936).

[28] L. J. Sham and M. Schluter, "Density-Functional Theory of the Energy Gap," *Phys. Rev. Lett.*, **51** [20] 1888–91 (1983).

[29] J. P. Perdew and M. Levy, "Physical Content of the Exact Kohn-Sham Orbital Energies: Band Gaps and Derivative Discontinuities," *Phys. Rev. Lett.*, **51** [20] 1884–87 (1983).

[30] J. D. Dow and D. Redfield, "Toward a Unified Theory of Urbach's Rule and Exponential Edges," *Phys. Rev. B: Condens. Matter*, **5** [2] 594–610 (1972).

[31] T. Tomiki, "Optical Constants and Excition States in KCl Single Crystalls. II The Spectra of Reflectivity and Absorption Constant," *J. Phys. Soc. Jpn.*, **23** [6] 1280–96 (1967).

[32] R. H. French, R. V. Kasowski, F. S. Ohuchi, D. J. Jones, H. Song, and R. L. Coble, "Band Structure Calculations of the High-Temperature Electronic Structure of MgO"; unpublished work.

[33] R. S. Knox, "Theory of Excitions" (Edited by F. Seitz, D. Turnbull, and H. Ehrenreich), *Solid State*

Phys., **5**, 1–194 (1963).

[34]M. Ueta, H. Kanzaki, K. Kobayashi, Y. Toyozawa, and E. Hanamura, "Excitonic Processes in Solids"; in Springer Series in Solid State Sciences, Vol. 60. Edited by M. Cardona, P. Fulde, K. von Klitzing, and H. J. Queisser. Springer–Verlag, New York, 1986.

[35]Y. Toyozawa, "Theory of Line-shapes of the Exciton Absorption Bands," *Prog. Theor. Phys.*, **20** [1] 53–81 (1958).

[36]M. Skibowski, G. Sprussel, and V. Saile, "Fine Structure and Temperature Dependence of Shallow Core Excitons in Insulators and Semiconductors," *Appl. Opt.*, **19** [23] 3978–86 (1980).

[37]J. C. Phillips, Bonds and Bands in Semiconductors. Academic Press, New York, 1973.

[38](see, for example) J. E. Huheey, Inorganic Chemistry, Principles of Structure and Reactivity; pp. 56–81. Harper and Row, New York, 1972.

[39]C. Kittel, Solid State Physics; p. 210. Wiley, New York, 1976.

[40]R. C. Hughes., "Generation, Transport, and Trapping of Excess Charge Carriers in Czochralski Grown Sapphire," *Phys. Rev. B: Condens. Matter*, **19** [10] 5318–28 (1979).

[41](a) C. Kittel, Solid State Physics; p. 313. Wiley, New York, 1976. (b) D. C. Langreth, "Polaron Mobility at Finite Temperature," *Phys. Rev.*, **159** [3] 717–25 (1967).

[42]J. M. Ziman, Principles of the Theory of Solids; p. 220. Cambridge University Press, New York, 1972.

[43]M. Tinkham, Group Theory and Quantum Mechanics; p. 210. McGraw–Hill, New York, 1964.

[44]R. H. French, R. L. Coble, R. V. Kasowski, and F. S. Ohuchi, "Vacuum Ultraviolet, Photoemission, and Theoretical Studies of the Electronic Structure of Al_2O_3 up to 1000°C" (in Proceedings of the International Conference on Electronic Structure and Phase Stability in Advanced Ceramics), *Physica B, (Amsterdam)*, **150**, 47–49 (1988).

[45]P. B. Allen and M. Cardona, "Temperature Dependence of the Direct Gap of Si and Ge," *Phys. Rev. B: Condens. Matter*, **27** [8] 4760–69 (1983).

[46]M. L. Cohen and D. J. Chadi, "Temperature Dependence of Semiconductor Band States"; pp. 155–80 in Handbook on Semiconductors, Vol. 2. Optical Properties of Solids. Edited by M. Balkanski. North-Holland, New York, 1980.

[47]N. Ishizawa, T. Miyata, F. Marumo, and S. Iwai, "A Structural Investigation of α-Al_2O_3 at 1900°C," *Acta Crystallogr., Sect. B: Struct. Sci.*, **B36**, 228 (1980).

[48]P. Aldebert and J. P. Traverse, "Neutron Diffraction Study of Structural Characteristics and Ionic Mobility of α-Al_2O_3 at High Temperatures," *J. Am. Ceram. Soc.*, **65** [9] 460 (1982).

[49]R. H. French and J. B. Blum, "Electronic Structure and Conductivity of Al_2O_3"; pp. 111–34 in Ceramic Transactions, Vol. 7. Sintering of Advanced Ceramics. American Ceramic Society, Westerville, OH, 1990.

[50]M. M. El-Aiat and F. A. Kroger, "Determination of the Parameters of Native Disorder in α-Al_2O_3," *J. Am. Ceram. Soc.*, **65** [3] 163–66 (1982).

[51]F. A. Kroger, "Electrical Properties of α-Al_2O_3"; pp. 1–15 in Advances in Ceramics, Vol. 10. Structure and Properties of MgO and Al_2O_3 Ceramics. Edited by W. D. Kingery. American Ceramic Society, Columbus, OH, 1984.

[52]K. Kitazawa and R. L. Coble, "Electrical Conduction in Single-Crystal and Polycrystalline Al_2O_3 at High Temperatures," *J. Am. Ceram. Soc.*, **57** [6] 245–50 (1974).

[53]J. H. Effert, K. A. Goettel, and I. F. Silvera, "Ruby at High Pressure I. Optical Line Shifts to 156 GPa," *Phys. Rev. B: Condens. Matter*, **40** [8] 5724–32 (1989).

[54]J. H. Effert, K. A. Goettel, and I. F. Silvera, "Ruby at High Pressure II. Fluorescence Lifetime of the R Line to 130 GPa," *Phys. Rev. B: Condens. Matter*, **40** [8] 5733–83 (1989).

[55]A. Jayaraman, "Ultrahigh Pressures," *Rev. Sci. Instrum.*, **57** [6] 1013–31 (1986).

[56]H. Song, R. H. French, and R. L. Coble, "Effect of Residual Strain on the Electronic Structure of Al_2O_3 and MgO," *J. Am. Ceram. Soc.*, **72** [6] 990–94 (1989).

[57]F. S. Ohuchi, "Metal–Ceramic Interfacial Reactions: A Surface Science Approach"; in Bonding, Structure, and Mechanical Properties of Metal/Ceramic Interfaces. Edited by A. G. Evans and M. Rühle. Pergamon Press, Elmsford, NY, 1990.

[58]F. S. Ohuchi and R. H. French, "Effect of Oxygen Incorporation in AlN Thin Films," *J. Vac. Sci. Technol. A*, **6** [3] 1695–96 (1988).

[59]F. S. Ohuchi and P. E. Russell, "AlN Thin Films with Controlled Crystallographic Orientations and Their Microstructure," *J. Vac. Sci. Technol. A*, **5** [4] 1630–34 (1987).

[60]F. S. Ohuchi, R. H. French, and R. V. Kasowski, "A Study of Room-Temperature Cu–Al_2O_3 and Cu–AlN Interfacial Interactions," *J. Vac. Sci. Technol. A*, **5** [4] 1175–77 (1987).

[61]F. S. Ohuchi, R. H. French, and R. V. Kasowski, "Cu Deposition on Al_2O_3 and AlN Surfaces: Electronic Structure and Bonding," *J. Appl. Phys.*, **62** [6] 2286–89 (1987).

[62]R. V. Kasowski, F. S. Ohuchi, and R. H. French, "Theoretical and Experimental Studies of Cu Metallization of Al_2O_3" (in Proceedings of the International Conference on Electronic Structure and Phase Stability in Advanced Ceramics), *Physica B, Amsterdam*, **150**, 44–46 (1988). □